ISSN 1066-3622, Radiochemistry, 2014, Vol. 56, No. 4, pp. 385–391. © Pleiades Publishing, Inc., 2014.
Published in Russian in Radiokhimiya, 2014, Vol. 56, No. 4, pp. 326–331.

Immobilization of Lanthanum, Cerium, and Selenium into Ceramic Matrix of Sodium Zirconium Phosphate[1]

A. Bohre*, K. Awasthi, and O. P. Shrivastava

Department of Chemistry, Dr. H.S. Gour University, Sagar. 470003 India
* *e-mail: ashish.bohre@gmail.com*

Received August 19, 2013; in final form, January 4, 2014

Abstract—The crystallographic nature of $NaCe_{0.2}Zr_{1.8}P_3O_{12}$, $NaSe_{0.2}Zr_{1.8}P_3O_{12}$, and $NaLa_{0.13}Ce_{0.14}Se_{0.15}Zr_{1.58}P_3O_{12}$ phases has been investigated with the aim of developing methods for radionuclide immobilization into sodium zirconium phosphate (NZP) phase. The phases have the NZP structure, space group $R\bar{3}c$, $Z = 6$. Powder diffraction data have been subjected to Rietveld refinement, and satisfactory structural convergence of *R*-factors was achieved. The PO_4 stretching and bending vibration bands in the IR region have been assigned.

Keywords: ceramic, lanthanum, cerium, selenium, NZP structures, powder X-ray diffraction, GSAS program, Rietveld refinement

DOI: 10.1134/S1066362214040055

The disposal of high-level radioactive waste generated during reprocessing of spent fuel from nuclear reactors to recover actinides is the subject of active research. Chemically and radiologically, reprocessed wastes are extremely complex in nature. They contain fission products, residual actinides, cations from dissolution of fuel rod containers, alkali salts, and a variety of organic compounds [1–3]. To reduce their volume and to stabilize their chemistry, reprocessed commercial wastes in the liquid form are often converted into a solid form by drying and calcining them at temperatures below 600°C. During calcination, the wastes decompose into amorphous mixtures of chemically inert oxides, while volatile reaction products are driven off. The solid products (or calcines) are characterized by moderate to high leachability and need to be converted to chemically stable form before they are finally disposed of [1, 4]. Therefore, the development of waste forms suitable for immobilization of reprocessed high-level calcines remains a challenging task for chemists. In response to this challenge, diverse waste forms including noncrystalline borosilicate glasses and crystalline and multiphase materials have been proposed.

Borosilicate glass is currently used for the fixation of high-level nuclear waste (HLW) in several nuclear power generating plants around the world [5]. The procedure involves the concentration of the nitrate waste solution obtained after reprocessing of the spent fuel and its addition to the mixture of glass-forming components consisting of boric acid, sodium carbonate, and silica. This results in the formation of slurry from which water and other volatile components are removed by slow heating, and the resulting oxides from the nitrates are incorporated in the glass matrix by heating the charge to the pouring temperature of glass which can be as high as 1150°C. During this process, oxides of several elements such as Cs, Te, Ru, etc., vaporize and are deposited in the ducts and pipelines connected to the processing plant, making this area inaccessible for work to the technicians, due to high radioactivity [6, 7]. It is therefore necessary to devise a process in which these elements could be fixed in a solid matrix at relatively low temperatures when the vaporization of these oxides is insignificant. The other disadvantage of fixing the radioactivity in glass is associated with its thermodynamically metastable nature. The solidified radioactive glass contained in special steel canisters located in the repositories can spontaneously devitrify, and the heat released in this process can breach the canister and expose its radioactive contents to the environment.

The sodium zirconium phosphate structural family (NZP), of which $NaZr_2(PO_4)_3$ is the parent composition, is well known for its ionic conductivity, low ther-

[1] The text was submitted by the authors in English.

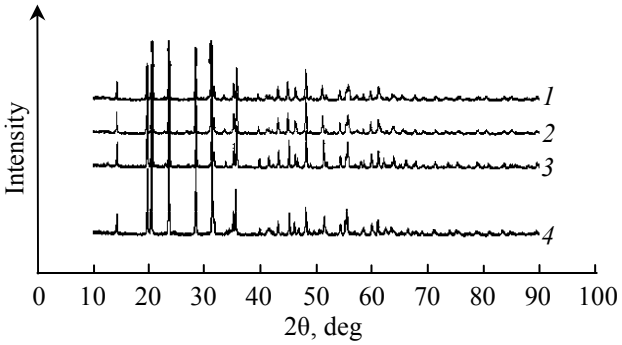

Fig. 1. Powder XRD patterns of (*1*) $NaLa_{0.13}Ce_{0.14}Se_{0.15}Zr_{1.58}P_3O_{12}$, (*2*) $NaZr_{1.8}Se_{0.2}P_3O_{12}$, and (*3*) $NaZr_{1.8}Ce_{0.2}P_3O_{12}$ ceramic samples and (*4*) of $NaZr_2P_3O_{12}$.

mal expansion [8, 9], and structural flexibility to accommodate a large number of multivalent ions [10]. The unique properties of NZP materials are attributed mainly to (a) an open framework structure with strongly bonded polyhedra, (b) flexibility with regards to ionic substitution, and (c) anisotropic thermal expansion of the lattice under thermal stress. In addition, this material has been extensively studied for use as a host ceramic for high-level nuclear waste immobilization. Furthermore, being the only known single-phase host structure exhibiting structural stability at high temperatures (even under radiation exposure) and low solubility in water in a wide pH range, NZP has been evaluated as a potential alternative to borosilicate glass and polycrystalline Synroc systems [11–13]. Orlova and coworkers studied by X-ray diffraction compounds of some *f* elements with structures of NZP and $CePO_4$ types [8, 14]. Volkov et al. examined the crystal structures and thermal expansion of monazite-like compounds of some tetravalent *f* elements [14, 15].

Here we demonstrate the principal feasibility of immobilizing lanthanum, cerium, and selenium in the NZP matrix using an acceptable structure model based on the refinement of crystallographic data. We also study the crystallochemical changes due to matrix modification when La^{3+}, Ce^{4+}, and Se^{4+} cations are substituted in the zirconium site of the NZP framework.

EXPERIMENTAL

Ceramic synthesis of $NaCe_{0.2}Zr_{1.8}P_3O_{12}$, $NaSe_{0.2}Zr_{1.8}P_3O_{12}$, and $NaLa_{0.13}Ce_{0.14}Se_{0.15}Zr_{1.58}P_3O_{12}$ phases. Solid solutions of $NaCe_{0.2}Zr_{1.8}P_3O_{12}$, $NaSe_{0.2}Zr_{1.8}P_3O_{12}$, and $NaLa_{0.13}Ce_{0.14}Se_{0.15}Zr_{1.58}P_3O_{12}$ were synthesized by the conventional solid-state method. Stoichiometric amounts of dry fine powders of the precursors were ground in a mortar in a glycerol medium. The selected precursors were AR grade $La(NO_3)_3$, Na_2CO_3, SeO_2, CeO_2, $ZrO(NO_3)_2$, and $(NH_4)H_2PO_4$. The glycerol paste was gradually heated initially at 600°C for 8 h in a platinum crucible. The initial heating is done to decompose $La(NO_3)_3$, Na_2CO_3, and $(NH_4)H_2PO_4$ with the emission of NO_x, CO_2, NH_3, and water vapor. The powders were then compacted into small discs 12.5 mm in diameter and 2–3 mm thick under a load of 4 t. Then the pellets were sintered in a platinum crucible at 1250°C for 72 h.

Characterization. The phase purity of the synthesized samples was checked by X-ray diffraction (XRD) on a PANalytical diffractometer (XPERT-PRO) using CuK_α radiation (λ = 1.54060 Å) at a step of $2\theta = 0.02°$ and a fixed counting time of 5 s per step. The structures were refined by the Rietveld method using the GSAS program. The homogeneity and chemical compositions of the samples were checked by scanning electron microscopy (SEM) using an electron microscope system (Zeiss) equipped with a Thermo Noran ultradry detector facility for energy-dispersive X-ray (EDAX) analysis. The images presented are recorded in the backscattered electron (BSE) mode at the electron energy of 20 keV. To confirm the functional compositions of the phosphates, their IR spectra were recorded using a Shimadzu FTIR-8400S instrument. Samples were prepared as KBr pellets.

RESULTS AND DISCUSSION

Rietveld refinement and crystallographic model of the phases. The powder XRD data showed that the single-phase samples of compositions $NaCe_{0.2}Zr_{1.8}P_3O_{12}$, $NaSe_{0.2}Zr_{1.8}P_3O_{12}$, and $NaLa_{0.13}Ce_{0.14}Se_{0.15}Zr_{1.58}P_3O_{12}$ were isostructural to $NaZr_2(PO_4)_3$ (Fig. 1). NZP crystallizes in the rhombohedral system (space group $R\bar{3}c$). The conditions for the rhombohedral lattice ($-h + k + l = 3n$; when $h = 0$, $l = 2n$; when $k = 0$, $l = 2n$) have been verified for all reflections in the 2θ range 10°–90°. The intensity and positions of the reflections in the diffraction pattern match with the characteristic pattern for the parent compound, sodium zirconium phosphate, which gives several prominent reflections in the 2θ range 13.98°–46.47° [16]. The general structure analysis system (GSAS) [17] program

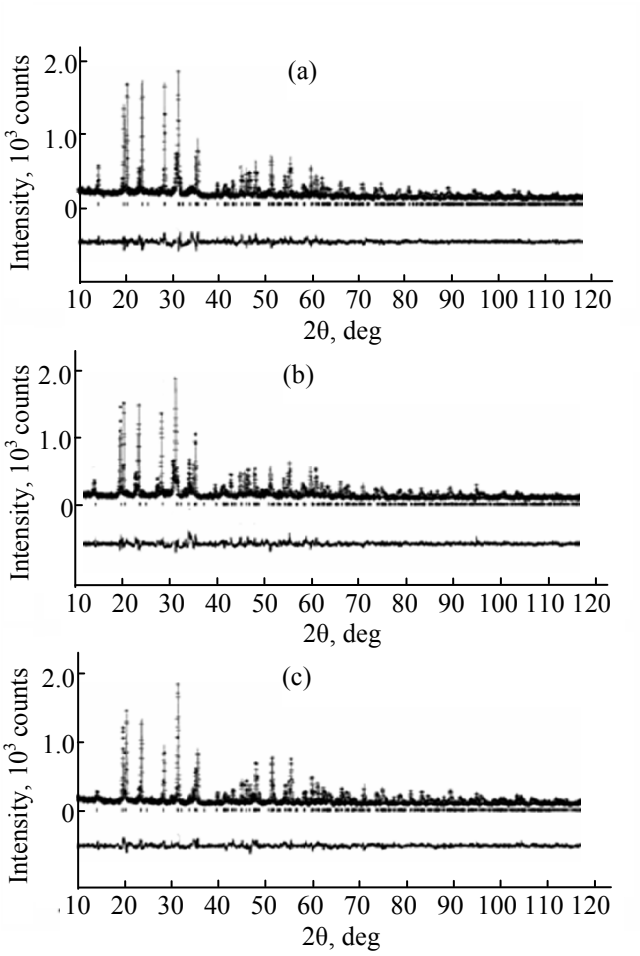

Fig. 2. Rietveld refinement plot for (a) $NaLa_{0.13}Ce_{0.14}Se_{0.15}Zr_{1.58}P_3O_{12}$, (b) $NaZr_{1.8}Se_{0.2}P_3O_{12}$, and (c) $NaZr_{1.8}Ce_{0.2}P_3O_{12}$ ceramic samples. Points are experimental data, curves are calculated, lower curves are differences between the experiment and calculation, and vertical bars are Bragg reflections of the crystalline phases.

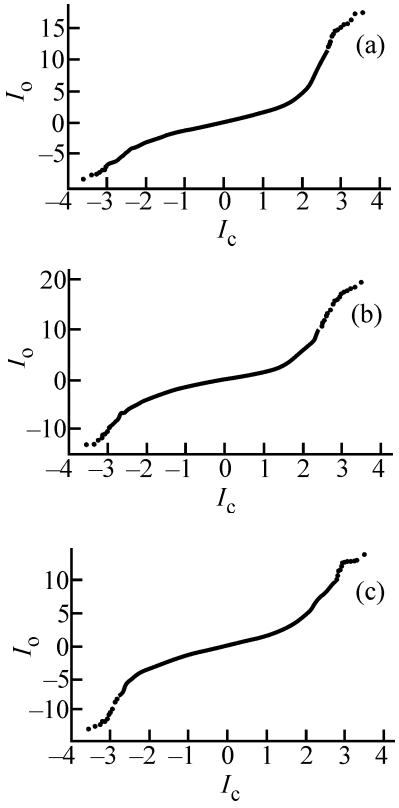

Fig. 3. Correlation between the observed (I_o) and calculated intensities (I_c) for (a) $NaLa_{0.13}Ce_{0.14}Se_{0.15}Zr_{1.58}P_3O_{12}$, (b) $NaZr_{1.8}Se_{0.2}P_3O_{12}$, and (c) $NaZr_{1.8}Ce_{0.2}P_3O_{12}$ ceramic samples.

with the EXPGUI [18] graphical user interface was used for Rietveld analysis [19] of the X-ray powder diffraction data. High quality powder diffraction data in combination with the Rietveld method allow refinement of the structural model (atomic coordinates, site occupancies, and atomic displacement parameters) as well as of profile parameters (lattice constants, peak shape and height, instrument parameters, and background).

The structure refinement leads to rather good agreement between the experimental and calculated XRD patterns (Fig. 2) and yields acceptable reliability factors: RF^2, R_p, and R_{wp}. The correlation between the observed and calculated intensities shows that the distribution is approximately normal (Fig. 3). The lattice parameters are close to the corresponding values for the unsubstituted NZP unit cell [20]. In contrast to the previously published data [21], the substitution of Zr^{4+} cation by tetravalent Se^{4+} and Ce^{4+} and trivalent La^{3+} cations causes elongation of the unit cell along *c* axis. Along the *a* axis, the unit cell shrinks (Table 1) [22]. Changes in the lattice parameters show that the framework modifies its dimensions to accommodate the cations without breaking the bonds [23]. The basic framework of NZP accepts cations of different sizes and oxidation states to form solid solutions with the overall geometry retained. The final atomic coordinates and isotropic thermal parameters (Table 2), interatomic distances (Table 3), and bond angles (Table 4) are extracted from the crystal information file (CIF) prepared after the final cycle of refinement. The refinement leads to acceptable Zr–O and P–O bond distances. Zr atoms are displaced from the center of the octahedron due to the Na^+–Zr^{4+} repulsions. The Zr–O(2) distance adjacent to the Na atom is slightly longer than the Zr–O(1) distance; however, the average Zr–O distances are smaller than the values calculated from the ionic radii (2.12 Å) [24]. Changes in the bond distances and bond angles with La/Ce/Se substitution

Table 1. Crystallographic data for $NaZr_{1.8}Ce_{0.2}P_3O_{12}$, $NaZr_{1.8}Se_{0.2}P_3O_{12}$, and $NaLa_{0.13}Ce_{0.14}Se_{0.15}Zr_{1.58}P_3O_{12}$ calcined ceramic phases at room temperature[a]

Parameter	$NaZr_{1.8}Ce_{0.2}P_3O_{12}$	$NaZr_{1.8}Se_{0.2}P_3O_{12}$	$NaLa_{0.13}Ce_{0.14}Se_{0.15}Zr_{1.58}P_3O_{12}$
$a = b$, Å	8.78546(12)	8.71648(17)	8.64857(21)
c, Å	22.7178(5)	22.7918(6)	22.8478(7)
R_p	0.0749	0.0796	0.0797
R_{wp}	0.1854	0.1144	0.1782
R_{exp}	0.0777	0.0870	0.0884
RF^2	0.14785	0.14897	0.18796
V_{cell}, Å^3	1573.31(4)	1570.82(7)	1559.67(9)
S (GoF)	2.145	2.458	2.478
DW_d	0.990	0.801	0.732
Unit cell formula weight	2854.532	2989.516	2904.500
D_x, d cm^{-3}	3.100	3.132	3.440
Slope	1.24	1.39	1.11

[a] Structure: rhombohedral, space group $R\bar{3}c$, $Z = 6$, $\alpha = \beta = 90°$, $\gamma = 120°$. $R_p = \sum(y_i^{obs} - y_i^{calc})/\sum y_i^{obs}$; $R_{wp} = [\sum w_i(y_i^{obs} - y_i^{calc})^2/\sum w_i(y_i^{obs})^2]^2$; $R_{exp} = [(N - P)/\sum w_i(y_i^{obs})^2]^{1/2}$; $S = R_{wp}/R_{exp}$; y_i^{obs} and y_i^{calc} are observed and calculated intensities at profile point i, respectively. w_i is the weight for each step i. N is the number of parameters refined.

Table 2. Refined atomic coordinates for $NaZr_{1.8}Ce_{0.2}P_3O_{12}$, $NaZr_{1.8}Se_{0.2}P_3O_{12}$, and $NaLa_{0.13}Ce_{0.14}Se_{0.15}Zr_{1.58}P_3O_{12}$ calcined ceramic phases at room temperature

Atom	x	y	z	Occupancy	U_{iso}, Å^2
$NaCe_{0.2}Zr_{1.8}P_3O_{12}$					
Na	0.0	0.0	0.0	1.0	0.04731
Ce	0.0	0.0	0.0	0.2	0.18517
Zr	0.0	0.0	0.13	1.0	0.01348
P	0.29347	0.0	0.25	1.0	0.01897
O(1)	0.17594	–0.02425	0.19	1.0	0.01543
O(2)	0.194	0.17051	0.08	1.0	0.05243
$NaSe_{0.2}Zr_{1.8}P_3O_{12}$					
Na	0.0	0.0	0.0	1.0	0.08731
Se	0.0	0.0	0.0	0.2	0.28517
Zr	0.0	0.0	0.13	1.0	0.03748
P	0.29347	0.0	0.25	1.0	0.02597
O(1)	0.17594	–0.02425	0.19	1.0	0.04843
O(2)	0.194	0.17051	0.08	1.0	0.07843
$NaLa_{0.13}Ce_{0.14}Se_{0.15}Zr_{1.58}P_3O_{12}$					
Na	0.0	0.0	0.0	1.0	0.08731
La	0.0	0.0	0.0	0.13	0.17817
Ce	0.0	0.0	0.0	0.14	0.21517
Se	0.0	0.0	0.0	0.15	0.18517
Zr	0.0	0.0	0.13	1.0	0.02748
P	0.9347	0.0	0.25	1.0	0.01597
O(1)	0.17594	–0.02425	0.19	1.0	0.03843
O(2)	0.194	0.17051	0.08	1.0	0.06843

can be clearly seen in the tables. The bond distances increase from 2.03 to 2.08 Å upon substitution of Zr by Ce/Se/La. The O–Zr–O angles vary between 89.97° and 175.79°. The angles between the shortest bonds are larger than those between the longest bonds because of the O–O repulsion which is stronger for O(1)–O(1) than for O(1)–O(2). The P–O distances are close to those found in NASICON type phosphates. The O–P–O angles vary in the range 105.50°–122.09°. The average Na–O (2.43 Å) and P–O (2.05 Å) distances are longer than in the previously published work [25]. We believe that selenium is in the 6-coordinate surrounding, although it is a matter of discussion because 4-coordinate tetrahedral state is also known when Se occupies phosphorus positions in NASICON type NZP-based materials. Figure 4 shows

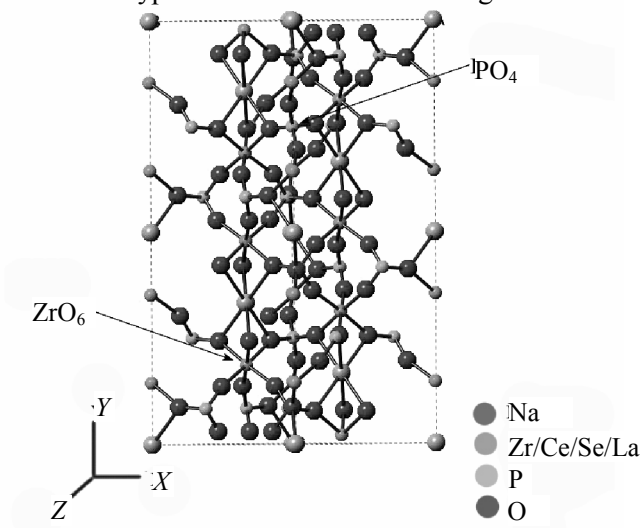

Fig. 4. Ball-and-stick view of $NaLa_{0.13}Ce_{0.14}Se_{0.15}Zr_{1.58}P_3O_{12}$ ceramic sample.

Table 3. Interatomic distances (Å) for $NaZr_{1.8}Ce_{0.2}P_3O_{12}$, $NaZr_{1.8}Se_{0.2}P_3O_{12}$, and $NaLa_{0.13}Ce_{0.14}Se_{0.15}Zr_{1.58}P_3O_{12}$ calcined ceramic phases at room temperature[a]

Bond	$NaZr_{1.8}Ce_{0.2}P_3O_{12}$	$NaZr_{1.8}Se_{0.2}P_3O_{12}$	$NaLa_{0.13}Ce_{0.14}Se_{0.15}Zr_{1.58}P_3O_{12}$
Na(1)–O(1) (×6)	2.47782(7)	2.7318(5)	2.37005(5)
Na(2)–O(2) (×2)	2.177985(7)	2.37964(5)	2.32960(5)
Zr/Ce/Se/La–O(1) (×3)	2.03158(30)	2.03796(30)	2.07492(30)
Zr/Ce/Se/La–O(2) (×3)	2.087486(30)	2.07894(30)	2.04878(30)
P–O(1) (×2)	1.517348(30)	1.515879(30)	1.78452(30)
P–O(2) (×2)	1.538475(30)	1.54894(30)	1.497853(30)

[a] Here and in Table 4, the estimated standard deviation is indicated in parentheses.

Table 4. Bond angles for $NaZr_{1.8}Ce_{0.2}P_3O_{12}$, $NaZr_{1.8}Se_{0.2}P_3O_{12}$, and $NaLa_{0.13}Ce_{0.14}Se_{0.15}Zr_{1.58}P_3O_{12}$ calcined ceramic phases at room temperature

Angle	$NaZr_{1.8}Ce_{0.2}P_3O_{12}$	$NaZr_{1.8}Se_{0.2}P_3O_{12}$	$NaLa_{0.13}Ce_{0.14}Se_{0.15}Zr_{1.58}P_3O_{12}$
O(1)−Na(1)−O(1) (×6)	63.3294(10)	66.4421(10)	67.4321(10)
O(2)−Na(1)−O(2)	180.0 (×2), 179.972	179.9802 (×3)	180.9802 (×3)
O(1)−Na(2)−O(1) (×5)	113.4701(10)	114.5548(10)	117.5648(10)
O(2)−Na(2)−O(2)	115.5196(10)	114.5187(10)	115.5387(10)
O(1)−Zr−O(1) (×3)	89.9784(8)	90.5488(9)	89.5148(9)
O(1)−Zr−O(2) (×3)	91.1288(9)	92.4725(9)	91.4975(9)
O(1)−Zr−O(2) (×3)	173.9482(10)	175.7909(10)	174.8609(10)
O(1)−Zr−O(2) (×3)	90.8749(9)	91.8578(9)	90.7578(9)
O(2)−Zr−O(2) (×3)	83.2489(9)	85.8738(9)	86.8788(9)
O(1)−P−O(1)	108.72497(12)	106.7189(12)	105.5079(12)
O(1)−P−O(2) (×2)	107.79190(10)	106.79140(10)	105.69140(10)
O(1)−P−O(2) ×2)	113.1487(5)	122.0972(5)	111.0972(5)

the ball-and-stick model demonstrating the ZrO_6 interribbon distance in the structure of the title phase, which is a function of the amount and size of alkali cation in the A site of the 3D framework built of ZrO_6 octahedra and corner-sharing PO_4 tetrahedra.

SEM and EDX analysis. The microstructure of the title phase was examined by SEM and EDAX analysis of the specimen. The morphology of SeNZP and CeNZP phase can be seen clearly in the electron micrographs of the ceramic sample (Fig. 5). Within the limits of the experimental error, the EDAX analytical data for Na, Zr, P, Se, La, and Ce are well consistent with the expected molar ratios.

IR analysis. The presence of orthophosphate anions in the crystal structure was confirmed by IR spectroscopy. The absorption bands in the range from 1280 to 1020 cm^{-1} are assigned to the stretching asymmetric vibrations ν_3, and bands in the range from 980 to 915 cm^{-1} correspond to the stretching symmetric vibrations ν_1 of the PO_4^{3-} ions. Bands in the range 670–400 cm^{-1} are assigned to the bending vibrations ν_4 and ν_2. Similar data have been reported by Barj et al. [26]. The IR data suggest that the compounds $NaCe_{0.2}Zr_{1.8}P_3O_{12}$, $NaSe_{0.2}Zr_{1.8}P_3O_{12}$, and $NaLa_{0.13}Ce_{0.14}Se_{0.15}Zr_{1.58}P_3O_{12}$ are orthophosphates (space group $R\bar{3}c$) [27–30] (Fig. 6).

Thus, refinement of powder X-ray diffraction data shows that the solid solutions of La-, Ce-, and Se-substituted sodium zirconium phosphate (NZP) prepared at 1250°C crystallize in the rhombohedral (space group $R\bar{3}c$) structure and do not exhibit any phase transition. The conditions for the rhombohedral lattice were verified for all reflections. The structure refinement suggests that La, Ce and Se are partially substituted for zirconium with the charge compensation acquired by incorporation of additional Na^+ ions. The crystal data and structural parameters of the material have been refined to satisfactory convergence with reasonable values of Rietveld parameters (R_p and R_{wp}). The calculated values of P–O and Zr–O bond lengths and O–M–O bond angles are in good agreement with the expected values. NZP is a promising material for

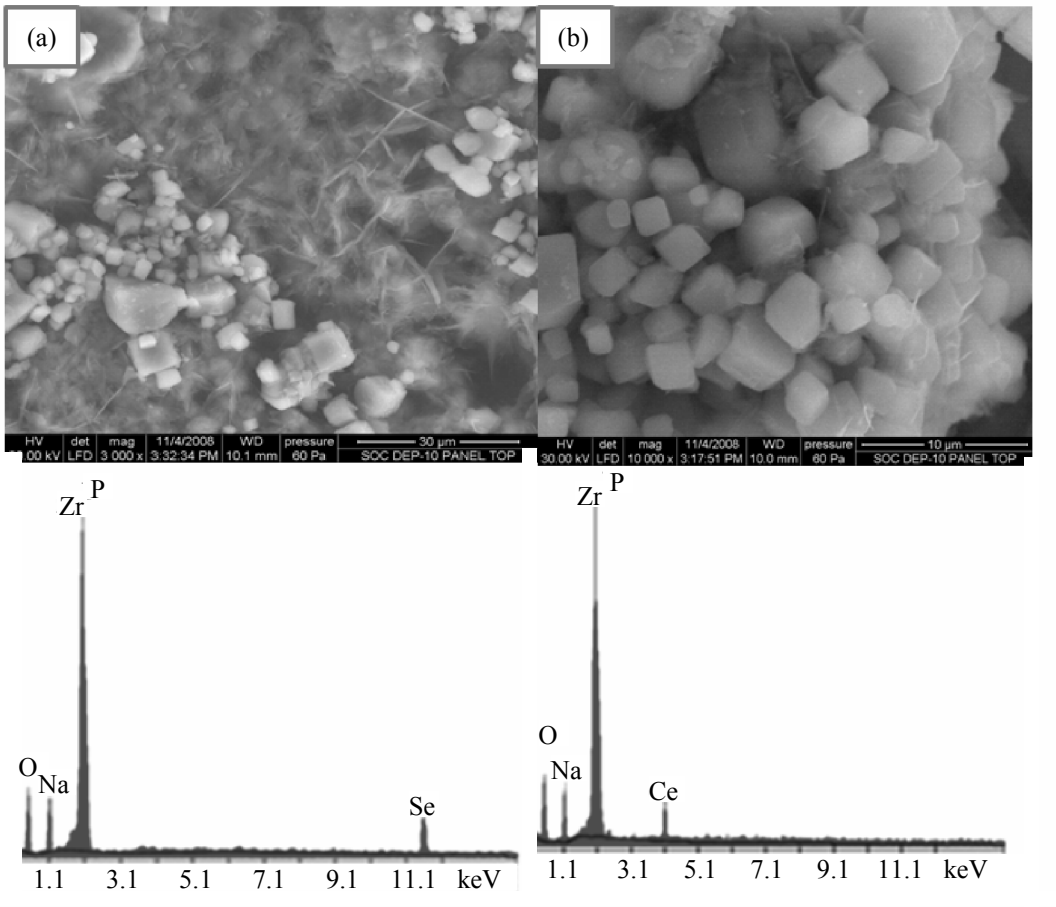

Fig.5. (a) Scanning electron micrographs and EDAX spectra of (a) $NaSe_{0.2}Zr_{1.8}P_3O_{12}$ and (b) $NaCe_{0.2}Zr_{1.8}P_3O_{12}$ ceramic phases.

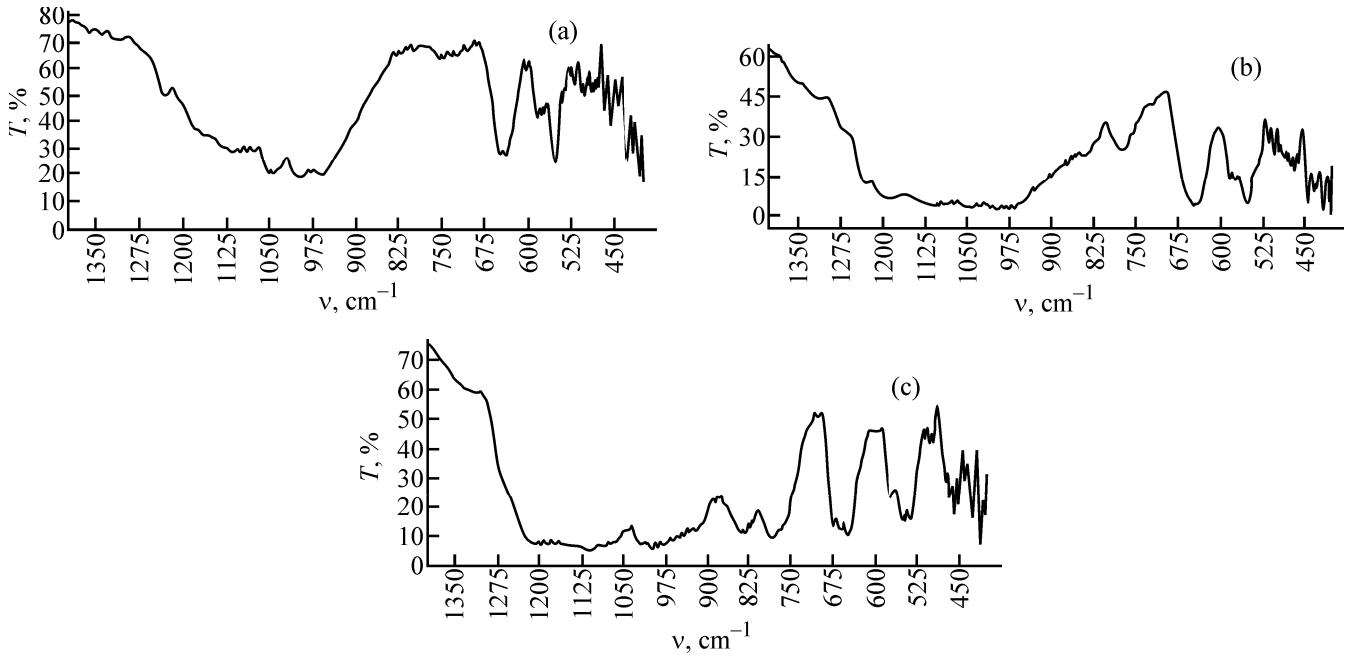

Fig. 6. IR spectra of (a) $NaLa_{0.13}Ce_{0.14}Se_{0.15}Zr_{1.58}P_3O_{12}$, (b) $NaZr_{1.8}Se_{0.2}P_3O_{12}$, and (c) $NaZr_{1.8}Ce_{0.2}P_3O_{12}$ ceramic samples.

immobilization and solidification of lanthanum, cerium, and selenium from intermediate-level waste from LWR fuel reprocessing.

REFERENCES

1. Donald, I.W., Metcalfe, B.L., and Taylor, R.N.J., *J. Mater. Sci*., 1997, vol. 32, pp. 5851–5887.
2. Li Wang and Tongxiang Liang, *J. Adv. Ceram*., 2012, vol. 1, no. 3, pp. 194–203.
3. Bohre, A. and Shrivastava, O.P., *Radiochemistry*, 2013, vol. 55, no. 4, pp. 442–449.
4. Bohre, A., Avasthi, K., Singh, B., and Shrivastava, O.P., *Radiochemistry*, 2014, vol. 56, no. 1, pp. 92–97.
5. Pratheep Kumar, S., Buvaneswari, G., Raja Madhavan, R., and Govindan Kutty, G.K.V., *Radiochemistry*, 2011, vol. 53, no. 4, pp. 421–429.
6. Bohre, A. and Shrivastava, O.P., *J. Nucl. Mater*., 2013, vol. 433, nos. 1–3, pp. 486–493.
7. Ringwood, A.E., Kesson, S.E., Ware, N.G., et al., *Nature*, 1979, vol. 278, pp. 219–223.
8. Bykov, D.M., Orlova, A.I., Tomilin, S.V., et al., *Radiochemistry*, 2006, vol. 48, no. 3, pp. 234–239.
9. Pet'kov, V.I., Sukhanov, M.V., and Kurazhkovskaya, V.S., *Radiochemistry*, 2003, vol. 45, no. 6, pp. 620–625.
10. Sales, B.C. and Boatner, L.A., *Mater. Lett*., 1984, vol. 2, no. 4, pp. 301–304.
11. Carter, M.L., Li, H., Zhang, Y., et al., *J. Nucl. Mater*., 2009, vol. 384, no. 3, pp. 322–326.
12. Scheetz, B.E., Agrawal, D.K., Breval, E., and Roy, R., *Waste Manag*., 1994, vol. 14, no. 6, pp. 489–505.
13. Roth, G. and Weisenburger, S., *Nucl. Eng. Des*., 2000, vol. 202, nos. 2–3, pp. 197–207.
14. Kitaev, D.B., Volkov, Yu.F., and Orlova, A.I., *Radiochemistry*, 2004, vol. 46, no. 3, pp. 211–217.
15. Volkov, Yu.F., Tomilin, S.V., Lukinykh, A.N., et al., *Radiochemistry*, 2002, vol. 44, no. 4, pp. 319–325.
16. JCPDS powder diffraction data file no. 71-0959. USA: Int. Center for Diffraction Data, 2000.
17. Larson, A.C. and Von Dreele, R.B., *LANSCE, MS-H805*, Los Alamos National Laboratory LAUR, 2000, no. 86-748.
18. Toby, B.H., *J. Appl. Crystallogr*., 2001, vol. 34, pp. 210–213.
19. Rietveld, H.M., *J. Appl. Crystallogr*., 1969, vol. 2, pp. 65–71.
20. Kojitani, H., Kido, M., and Akaogi, M., *Phys. Chem. Miner*., 2005, vol. 32, no. 4, pp. 290–294.
21. Orlova, A.I., Kitaev, D.B., Kazantsev, N.G., et al., *Radiochemistry*, 2002, vol. 44, no. 4, pp. 326–331.
22. Verissimo, C., Garrido, F.M.S., Alves, O.L., et al., *Solid State Ionics*, 1997, vol. 100, pp. 127–134.
23. Lenain, G.E., McKinstry, H.A., Alamo, J., and Agrawal, D.K., *J. Mater. Sci*., 1987, vol. 22, no. 1, pp. 17–22.
24. Hagman, L. and Kierkegaard, P., *Acta Chem. Scand*., 1968, vol. 22, pp. 1822–1832.
25. Shannon, R.D., *Acta Crystallogr., Sect. A*, 1976, vol. 32, pp. 751–767.
26. Barj, M., Perthuis, H., and Colomban, Ph., *Solid State Ionics*, 1983, vols. 9–10, pp. 845–850.
27. Borovikova, E.Yu., Kurazhkovskaya, V.S., Bykov, D.M., and Orlova, A.I., *J. Struct. Chem*., 2010, vol. 51, pp. 40–44.
28. Pet'kov, V.I., Asabina, E.A., Markin, A.V., and Smirnova, N.N., *J. Therm. Anal. Calorim*., 2008, vol. 91, pp. 155–160.
29. Buvaneswari, G. and Varadaraju, U.V., *J. Solid State Chem*., 1999, vol. 145, pp. 227–234.
30. Mbandza, A., Bordes, E., and Courtine, P., *Mater. Res. Bull*., 1985, vol. 20, pp. 251–257.